Journal of Membrane Science 444 (2013) 127–138

Contents lists available at SciVerse ScienceDirect

Journal of Membrane Science

journal homepage: www.elsevier.com/locate/memsci

Conductometric and computational study of cationic polymer membranes in H^+ and Na^+-forms at various hydration levels

Larisa V. Karpenko-Jereb [a,*], Anne-Marie Kelterer [a,**], Ninel P. Berezina [b], Alexander V. Pimenov [c]

[a] Institute of Physical and Theoretical Chemistry, Graz University of Technology, Graz, Austria
[b] Membrane Technology Institute, Kuban State University, Krasnodar, Russia
[c] Sankt-Petersburg University, Sankt-Petersburg, Russia Carbon NWC, S-Petersburg, Russia

ARTICLE INFO

Article history:
Received 18 December 2012
Received in revised form
3 May 2013
Accepted 8 May 2013
Available online 16 May 2013

Keywords:
Ion-exchange membrane
Microheterogeneous two-phase model
Molar conductivity
Diffusion coefficient
Quantum chemical calculation
Binding energy

ABSTRACT

Knowledge of the correlation between the molecular polyelectrolyte structure of membranes and their transport properties helps to develop new ion-exchange polymers with improved characteristics. This research paper studies the transport properties of two counter-ions, H^+ and Na^+, inside four commercial cationic membranes with experimental methods: three aromatic hydrocarbon polymer membranes CM-1, CMX, MK-40, and one tetrafluoroethylene polymer Nafion analog membrane MF-4SK. Ab initio calculations of the membrane structures with various hydration levels were applied in order to interpret the difference in the transport parameters of counter-ions between aromatic hydrocarbon MK-40 and non-aromatic perfluorinated MF-4SK polymer membranes. The membrane physico-chemical characteristics and the conductivity were experimentally investigated as a function of NaCl and HCl aqueous solution concentration. The conductivity and diffusion coefficients of the counter-ions, as well as volume fractions of 'gel' and 'inter-gel' phases were determined based on the microheterogeneous two-phase model. For the first time, ab initio calculations on membrane models were correlated with experimental findings in order to explain the difference in the mobility of the two counter-ions. The static ab initio study indicates the dissociation of the functional groups and a stronger water connectivity in perfluorinated membrane, providing an explanation for the measured highest diffusion coefficient and molar conductivity of the counter-ions H^+ and Na^+ in MF-4SK membrane in comparison to MK-40 membrane.

1. Introduction

At the present time ion-exchange membranes (IEMs) are finding very wide applications in different processes and devices: electro-dialysis, electrochemical synthesis, fuel cells, membrane bio-reactors, sensors, artificial organs, etc. [1–7]. In most applications the cationic membranes are found in Na^+ or H^+ -forms, or its mixture. Investigation of the interaction between the structural features and electro-transport characteristics of the membranes gives a better understanding of how they operate, and helps to develop new polymer materials with required properties. Numerous papers are dedicated to experimental and computational investigations of the correlation between the microstructure, the morphology of ion-exchange membranes, and its transport characteristics [7–31]. Koter et al. [8] investigated the influence of the length of the cross-linking chain in sulfinated and sulfonated polysulfone (PSU) on their physical and electro-transport properties in different aqueous electrolyte solutions. The cross-agent structure has been observed to have some effect on the counter-ion diffusion coefficient, but only a slight influence on conductivity and transport number. Saito et al. [9] investigated the conductivity, water transfer coefficient and water permeability of the commercial perfluorosulfonated membranes Nafion, Aciplex and Flemion in HCl, LiCl and NaCl aqueous solutions. The membrane conductivity increased with the increasing water content, and the H^+-form of the membranes possessed considerably higher conductivity than the membranes in Li^+ and Na^+-forms. Brandell et al. [10] concentrated their attention on the influence of the side-chain's length of perfluorinated membranes on the membrane transport characteristics. Using the Molecular Dynamics (MD) method, the researchers investigated the different side-chain lengths of Nafion, Dow and Aciplex at two different hydration levels (5 and 15 mol H_2O/mol SO_3). It was shown that at a high level of hydration, Nafion exhibits the highest mobility of water,

* Corresponding author. Tel.: +43 316 873 32241; fax: +43 316 873 32202.
** Corresponding author. Tel.: +43 316 873 32244; fax: +43 316 873 32202.
E-mail addresses: larisa.karpenko-jereb@tugraz.at (L.V. Karpenko-Jereb), kelterer@tugraz.at (A.-M. Kelterer), ninel_berezina@mail.ru (N.P. Berezina), pimenovalexandr@carbon-nwc.com (A.V. Pimenov).

0376-7388/$ - see front matter © 2013 Elsevier B.V. All rights reserved.
http://dx.doi.org/10.1016/j.memsci.2013.05.012

hydronium ion and the side-chain. Through the use of density functional calculations, Kim et al. [11] theoretically investigated the distribution of electron density in sulfonated polyarylenes containing flourine atoms in their backbones. They showed that the inclusion of short electron-withdrawing –CF_2–and –CF_2–CF_2– groups between the aromatic rings increases the acidity of the sulfonic acid group, and hence the conductivity of the proton. In a molecular dynamic study of SPEEK and Nafion, Mahajan and Ganesan [12] demonstrated that the sulfonate anion in SPEEK has a stronger basicity than Nafion. Idupulapati et al. [13] carried out the computational investigation of proton dissociation in four ionomer acids based on a different polymer matrix: perfluoro sulfonic (Nafion), perfluoro sulfonyl imide, aromatic sulfonyl imide and sulfonated polyetherether keton (SPEEK). They established that SPEEK requires six water molecules for proton dissociation, while perfluoro sulfonic and perfluoro sulfonyl imide acids need only three. They assumed that the presence of fluorine in the pendant chain of the ionomer membranes causes a substantial electron withdrawing effect, and therefore the sulfonic acid group has stronger acidic properties. Tsuda et al. [14] also found a dissociation of –SO_3H in Nafion membrane at hydration level ≥3. Using quantum chemical calculations, Spohr et al. [15] investigated the correlation between proton mobility and the degree of proton confinement in proton-carrying clusters near $-SO_3^-$-groups. They found that proton mobility increases with the increasing delocalization of the counter-charge, which is distributed on/over the polymer side chains. Furthermore, some investigations indicate the important role of the connectivity of water molecules with the membrane polymer matrix on the electro-transport characteristics of the ion-exchange membranes [19,24,26].

The aim of this work was to study the influence of the polymer morphology of cation-exchange membranes on the thermodynamic state of water and the transport characteristics of counter-ions (Na^+ and H^+). For this purpose the following investigations of the commercial sulfo-cationic membranes CM-1, CMX, MF-4SK and MK-40 with different chemical structures were carried out:

1) Experimental measurements of the physico-chemical characteristics and concentration dependencies of the conductivity of CM-1, CMX, MF-4SK and MK-40 membranes in NaCl and HCl aqueous solutions.
2) Estimations of the structural parameters and transport characteristics (diffusion coefficient and molar conductivity) of Na^+ and H^+ in the membranes from the obtained experimental data within the framework of the microheterogeneous two-phase model.
3) Computational calculations of the structures of MF-4SK and MK-40, as well as the binding energy (BE) of water molecules in these two membranes in Na^+ and H^+-forms at various hydration levels (0 up to 8 (10—for H^+-form of MF-4SK)). Models of the perfluorosulfonated membrane with a linear structure containing fluorine atoms in the polymer matrix, and of the hydrocarbonic aromatic polystyrene membrane with a branched polymer matrix were chosen in order to describe the main physico-chemical characteristics of the experimentally investigated membranes.
4) Analysis of the influence of the membrane structural features on the water binding energy and transport characteristics of Na^+ and H^+.

This paper combines for the first time experimental findings with quantum mechanical calculations to explain the difference in the transport parameters and mobility of two counter-ions in two different types of membranes.

2. Objects

Four commercial sulfocationic polymer membranes (MF-4SK, MK-40, CM-1 and CMX) were investigated experimentally. The manufacturers, synthesis method and chemical composition of the investigated membranes have been compiled in Table 1. The perfluorinated membrane MF-4SK consists of the saponified copolymer of sulphonyl fluoride vinylether and tetrafluoroethylene. The perfluorinated membrane MF-4SK is a homogeneous film without any cross-agent, and contains charged groups at the ends of the side segments of the fluoroethylene matrix. The basic structure of these ionomer membranes is shown in Fig. 1a. We should note that membrane MF-4SK has the same chemical structure and characteristics as membrane Nafion-117. The physico-chemical properties of the two membranes are not very different from each other, thus for MF-4SK: $Q=0.86$ mg-eqv/g_{dry},

Table 1
Manufacturer, synthesis method, chemical composition of the membranes.

Membrane	MF-4SK	MK-40	CM-1	CMX
Manufacturer	Plastpolymer Ltd., Russia	Azot Ltd., Russia	Tokuyama Corp., Japan	
Synthesis	Heat cast	Heat forge-rolling	"Paste" method	
Backing	Tetrafluorethylene	Polystyrene	Poly(vinyl chloride)	
Crosslinking	None	Divinylbenzene	Divinylbenzene	
Reinforcing	None	Polyamide (nylon cloth)	Poly(vinyl chloride)	

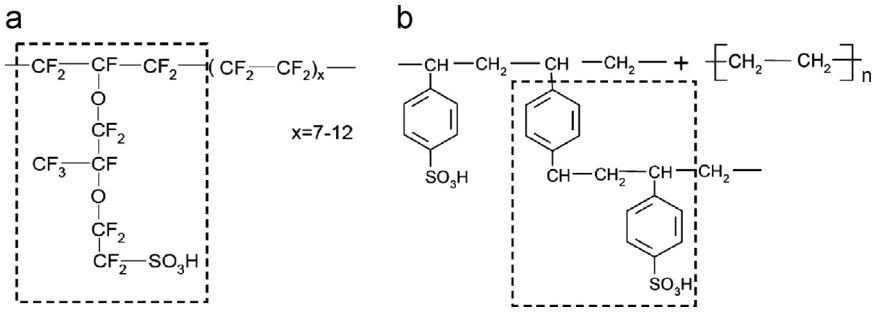

Fig. 1. Chemical structure of the membranes: (a) MF-4SK and (b) MK-40. The membrane models used in the quantum chemical calculations are marked by the squares.

$W=18.88\%$, $\kappa(0.1\ M\ NaCl)=6.40\times10^{-3}$ S/cm; for Nafion-117 [32]: $Q=0.93$ mg-eqv/g_{dry}, $W=18.95\%$, $\kappa(0.1\ M\ NaCl)=9.10\times10^{-3}$ S/cm. Membrane MK-40 has a polymer composition consisting of ion-exchange resin KU-2*8, high-pressure polyethylene as an inert polymer binder, and nylon cloth which is used as the reinforcing material. The sulfonic acid cation-exchange resin KU-2 is obtained by copolymerization of styrene and divinylbenzene, with the subsequent introduction of the sulfonic acid groups into the polymer matrix. The chemical structure of MK-40 is presented in Fig. 1b. The membranes CM-1 and CMX are made by creating a mixture of styrene, divinylbenzene and poly(vinyl chloride) (PVC) and pasting it onto a PVC support with consecutive thermal polymerization and post-sulfonation. Membrane CMX contains more poly(vinyl chloride), which makes its polymer chains longer than those of membrane CM-1. The ion-exchange capacity is correspondingly lower.

3. Methods

3.1. Membrane pre-treatment

The membranes MK-40 and MF-4SK were conditioned in accordance with the technique described in [33], after which they were kept in Na^+-form. The membranes CM-1 and CMX were conditioned and transported into 0.5 M NaCl, therefore these membranes were immediately brought to equilibrium with the NaCl solution. Before the resistance measurements, the membrane samples in Na^+-form were equilibrated with NaCl solutions for each concentration. The equilibrium establishment procedure is very important for obtaining reproducible results. According to the studies [34,35], the equilibrium establishment time depends on the solution concentration, the membrane type and sample size, and the conditions of obtaining equilibrium (stagnant, shaking, solution circulation). The establishment of the equilibrium between the membrane sample and the electrolyte solution was thoroughly monitored by conductometry. The equilibrium was considered established if the solution resistance above the membranes was the same as the resistance of the initial bulk solution. Depending on the concentration of the solution in stagnant conditions, the membranes were balanced within 24–70 h. 70 h were usually needed in order to reach the ionic equilibration between heterogeneous MK-40 membrane and diluted NaCl or HCl solutions (with concentrations 0.001–0.010 M).

For the investigation of ion-exchange capacity and membrane conductivity in HCl solutions, the membranes were transformed from Na^+-form to H^+-form through a 48 h immersion in 2 M HCl solution. After immersion the membranes were thoroughly washed in distilled water. The washed membrane samples (without the absorbed HCl solution) were then used for the determinations of ion-exchange capacity, water uptake and density. Before the resistance measurements, the membranes were equilibrated with an HCl solution of the respective concentration.

3.2. Ion-exchange capacity

(Q) was determined for H^+-form samples by titration of the H^+-ions produced during alkaline neutralization by KOH.

3.3. Water-uptake (W)

The total amount of water inside the membrane was determined by the gravimetric method. The membrane samples were weighed once after complete swelling in water, and then again after dehydration. The dehydration was maintained for 2–3 days at 105 °C until the weight of the sample did not change any more. The water uptake was determined as the mass ratio of absorbed water to dry membrane.

3.4. Density

Measurements were carried out on the water-swollen membrane samples using the gravimetric method.

3.5. Conductivity

The conductivity of the IEMs was measured by the mercury-contact method using alternating current (AC) of a high frequency (50–200 kHz) [35,36]. The schema of the test cell and electrical circuit of the method are presented in Fig. 2. When measuring the resistance of the membrane, the AC frequency was chosen so that the phase angle, which characterized the imaginary part of the impedance of mercury/membrane, was equal to zero. The specific membrane conductivity κ_m was calculated from the measured resistance by the following equation:

$$\kappa_m = \frac{l}{RS} \tag{1}$$

where l is the membrane thickness; R is the resistance; S is the area of membrane samples, which contact with mercury electrodes, in our measurement $S=0.785$ cm^2.

3.6. Computational methods

In order to study the influence of polymer morphology on the water connectivity of the membrane, we chose two different types of membranes: MF-4SK and MK-40. The computational investigation was made on models of these two membranes as shown in the squares of Fig. 1. The model of MF-4SK consists of the pristine side chain [–OF_2–CF–(CF_3)–O–CF_2–CF_2–SO_3–counter-ion] attached to the backbone, which has been reduced to [CF_3–CF–CF_3]. The model of MK-40 is represented by the polymer fragment [C_6H_5–CH(CH_3)–CH_2–CH_2–C_6H_4–SO_3–counter-ion].

The membrane models were investigated with Na^+ and H^+ counter-ions in their dry state and at various levels of hydration. The number of water molecules connected to the end group was varied from 1 to 10 for MF-4SK in H^+-form, and from 1 to 8 for MF-4SK in Na^+-form and MK-40 in H^+ and Na^+-forms.

The geometries were optimized using the Restricted Hartree Fock (RHF) method, with the 6–31+G (d,p) basis set [37] and tight optimization criteria. As recommended by Paddison [38] for the calculation of binding energy in such membranes diffuse functions were included in the basis set for the ionic system. For the geometries with 1–10 water molecules there exists a large variety of possible conformations on the potential energy surface. During this research the minimum search was performed by successively adding water molecules one by one, starting with different positions of the water molecules relative to the $-SO_3^-$ group of dry membranes. For the membrane models with one water, three possible starting geometries were used where water interacted

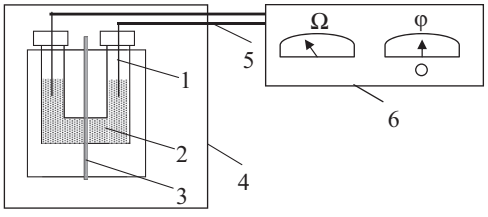

Fig. 2. Scheme of the mercury-contact method used to measure the membrane resistance: 1—Pt-electrodes; 2—mercury; 3—membrane sample; 4—air thermostat; 5—shielded copper cables; 6—impedance-meter Tesla VM-507.

with each of the three S=O groups. The geometries were then minimized and the binding energies were computed. During the next search step the lowest energy conformation was taken as the starting point. The potential energy surface for 1–3 water molecules was scanned as completely as possible. From the geometries with 2 and 3 water, the farthest water molecule from the $-SO_3^-$ group was deleted and one water molecule added closer to the $-SO_3^-$ group, either on the other side of the $-SO_3^-$ group or below the $-SO_3^-$ group. This modified structure was then optimized, and the binding energy was again computed. However, for the clusters with 4–10 waters, only 2–5 different conformations were optimized within this strategy with the restriction of a non-complete potential energy search. The quality of minima was checked via frequency analyses.The conformation with the lowest binding energy was then taken into account for the further interpretation of data.

The calculation of the binding energy of the membrane-water complexes was carried out using the local pair natural orbital-coupled-electron pair approximation (LPNO-CEPA/1) with the def2-TZVP basis set [39]. The LPNO-CEPA/1 method was referenced in order to accurately describe weak interactions [40]. For example, the interaction energy of the reaction $[H_3O^+ \ldots H_2O \rightarrow H_3O^+H_2O]$ was calculated to be only −0.02 kcal/mol smaller with the used method (LPNO-CEPA/1 energies without BSSE for CCSD(T)/quadruple zeta geometries) than with the reference W2 method (33.68 kcal/mol). Therefore, no basis set superposition error (BSSE) was taken into account in our computations of binding energies. The computational study was carried out using the program ORCA [41].

The binding energy E_B was computed from the electronic energy values (E) of the dry and hydrated membranes by the following expression:

$$E_B = E_{cluster} - E_{dry} - XE_{H_2O} \quad (2)$$

where X is the number of water molecules in the hydrated membrane; $E_{cluster}$, E_{dry}, E_{H_2O} are the electronic energies of the hydrated membrane with X water molecules, the dry membrane and one water molecule, respectively. In order to compare the different clusters, the binding energy per water molecule E_B/X was then computed and will be discussed in the Results section.

4. Theoretical approaches

4.1. Determination of the volume fractions of phase and 'free'- water in the swollen ion-exchange membrane

In order to analyze IEM conductivity data, the theoretical approach within the microheterogeneous two-phase model was applied [42,43]. Fig. 3 shows the schematic structure of a heterogeneous ion-exchange membrane swollen in an electrolyte solution. The heterogeneous IEM consists of the following microphases (pseudo-phases): (1) inert polymer; (2) polymer chains of ion-exchange polymer; (3) hydrated functional groups; (4) absorbed electrolyte (electroneutral) solution. The inert polymer and polymer chains of the ion-exchange polymer form the hydrophobic domains in the membrane. Homogeneous membranes contain no inert polymer in comparison to the heterogeneous membranes. The hydrated functional groups build the gel regions. The absorbed electroneutral solution is generally situated in the central part of the membrane pores (as shown in Fig. 3 reprinted from [44]). In order to describe the concentration dependencies of IEM conductivity within the framework of the microheterogeneous two-phase model, the IEM is divided into two microphases: (1) 'gel' phase (joint phase of the hydrophobic domains and the gel regions) and (2) 'inter-gel' spaces (or ´free´ solution)

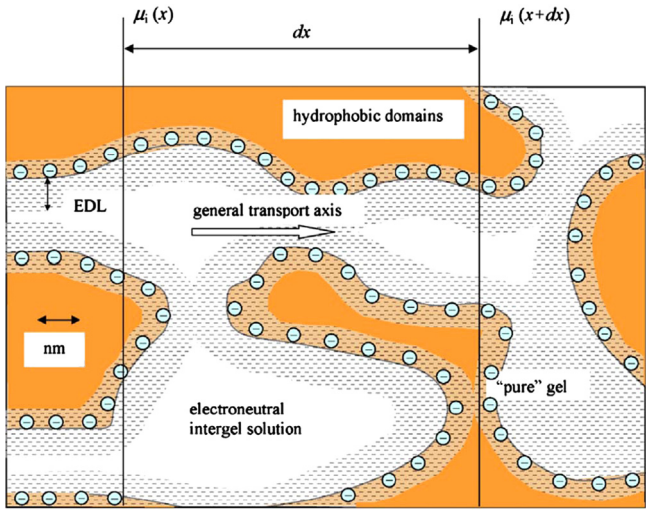

Fig. 3. Scheme representation of the ion-exchange membrane structure in nanometer scale in accordance with the microheterogeneous model. Hydrophobic domains are constituted by polymer chains devoid of fixed ion groups; the parts of chains bearing fixed ions form "pure" gel regions together with the charged electrical double layer (EDL) of the inner solution; the central zone of the pores is filled with the electroneutral intergel solution (Reprint from Larchet et al. [44] with permission from Elsevier).

containing absorbed electrolyte solution. If an IEM is equilibrated with pure water, the 'inter-gel' spaces are filled by non-bound water (so-called 'free' water), whose properties are similar to the properties of bulk water. The experimental and structural investigations [7,45–48] have proven the presence of non-bound water in ion-exchange membranes.

According to the first approximation normally used when applying the microheterogeneous two-phase model, the conductivity of the 'gel' phase does not depend on the equilibrium electrolyte concentration. However, the conductivity of the 'inter-gel' spaces does depend on it. The concentration dependencies of IEM conductivity are described by the following equation [42,43]:

$$\kappa_m^{\alpha} = f_1 \bar{\kappa}^{\alpha} + f_2 \kappa_{sol}^{\alpha} \quad (3)$$

where $\bar{\kappa}$ is the conductivity of the 'gel' phase; κ_{sol} is the conductivity of the equilibrium solution; f_1 and f_2 are the volume fractions of the phases. α reflects the reciprocal arrangement of the phases $-1 \le \alpha \le +1$. The size of the volume fraction f_2 of the equilibrium solution also indicates the heterogeneity degree of the membrane. At chaotic layout $\alpha \rightarrow 0$, Eq. 3 is rearranged into the expression

$$\kappa_m = \bar{\kappa}^{f_1} \kappa_{sol}^{f_2} \quad (4)$$

The conductivity of the 'gel' phase is determined as conductivity at the iso-conductance point, where the conductivity of the electrolyte solution is equal to the conductivity of the 'gel' phase and the membrane $\kappa_m = \kappa_{sol} = \bar{\kappa}$. According to this microheterogeneous two-phase model, the volume fraction of the 'inter-gel' phase (f_2) is easily defined as the slope from the bi-logarithmic dependence ($\lg\kappa_m$–$\lg\kappa_{sol}$)

$$f_2 = d\lg\kappa_m / d\lg\kappa_{sol} \quad (5)$$

The volume fraction of the 'gel' phase is equal to $f_1 = 1 - f_2$. As shown in the work of Brik et al. [48], the magnitudes of the volume fractions of the 'inter-gel' phase determined from concentration dependencies of the membrane conductivity using Eq. (5) are comparable to the values determined by contact etalon porometry and differential scanning calorimetry.

4.2. Diffusion coefficient of counter-ions

In the membrane 'gel' phase can be estimated from the membrane conductivity at the iso-conductance point. The diffusion coefficient can be calculated using the Nernst–Einstein equation adapted for polyelectrolytes [49]

$$\overline{D} = \overline{\kappa} \cdot \frac{RT\overline{t}}{F^2 z} \frac{f_1}{Q} \tag{5}$$

where R is the gas constant (8.314 J/(mol K)); F is the Faraday constant (96484.56 C/mol); T is the absolute temperature (298.15 K); Q is the ion-exchange capacity (mol/cm^3); z is the charge of counter-ion; f_1 is the volume fraction of the 'gel' phase; $\overline{t}$ is the transport number of a counter-ion in the membrane (proposed as $\overline{t}=1$). Larchet et al. [50] experimentally measured the true transport numbers of the counter-ions of different ion-exchange membranes (including MF-4SK and CM-2 with very close properties to CM-1). It was shown that at equilibrium, electrolyte concentration equal to or less than 1 M $\overline{t}$ is very close to 1. This fact proves the approximation $\overline{t}=1$.

4.3. Molar conductivity of counter-ions in 'gel' phase

Can be received via the following equation:

$$\overline{\lambda} = \overline{\kappa}/Q \tag{6}$$

4.4. Hydration capacity of membrane 'gel' phase.

The number of water molecules per functional group in the membrane 'gel' phase is determined by the volume fraction of the 'inter-gel' phase (f_2), the water uptake (W), and the ion-exchange capacity (Q) according to [51]

$$\overline{n} = \frac{1}{QM_{H_2O}} \left(W - f_2 \frac{d_{H_2O}}{d_m} \right) \tag{7}$$

The hydration capacity shows how many water molecules are bound to one $-SO_3^-$ group in the membrane 'gel' phase.

4.5. Applicability of the microheterogeneous two-phase model.

The approach of the microheterogeneous two-phase model has been widely applied in order to study the numerous labour-made, commercial membranes, including homogeneous perfluorinated membranes as well as membrane characterisations [24,50–59]. In this research paper we apply the microheterogeneous two-phase model for a comparison analysis of the conducting properties of commercial membranes in order to find out the influence of the polymer matrix on the mobility of the counter-ions in the 'gel' phase. The volume fraction of the 'inter-gel' phase can depend on the functional group concentration [28,51], as well as the method of membrane preparation [53] and pre-treatment [60]. As mentioned above, the conductivity of the 'inter-gel' phase depends on the equilibrium electrolyte solution concentration, which complicates the choice of one concentration for the correct comparison of the conductivity of different membranes. Since the conductivity of the membrane 'gel' phase does not depend on the concentration of the equilibrium electrolyte solution, in this paper the investigated membranes are compared according to the properties of the membrane 'gel' phase (hydration capacity of the membrane 'gel' phase, iso-conductance, diffusion coefficient and molar conductivity of counter-ions in the 'gel' phase).

5. Results and discussion

5.1. Experimental results

The physico-chemical characteristics such as water uptake (W), ion-exchange capacity (Q) and density (d_m) of the commercial membranes in H^+ and Na^+-forms are presented in Table 2. The water uptake for all membranes is somewhat higher in the H^+-form than the Na^+-form. Correspondingly, the density is lower in the H^+-form than the Na^+-form. The membrane MK-40 possesses the highest water uptake, while MF-4SK demonstrates the lowest in both H^+ and Na^+ ionic forms. The density of the swollen and dry MF-4SK membrane is approximately 30% larger than the density of the other investigated membranes.

Fig. 4 displays the dependencies of the specific membrane conductivity κ_m on the concentration of equilibrium electrolyte solutions NaCl (Fig. 4a) and HCl (Fig. 4b). The comparison of Fig. 4a and b shows that the conductivity of all membranes is substantially higher in HCl than in NaCl solutions, because the protons possess significantly higher mobility than the sodium ions. The proton's higher mobility is in large part due to the fact that it is transported via two mechanisms: structural diffusion (Grotthuss mechanism) and mass diffusion (vehicular mechanism) [30,31], whereas the sodium ion is only transferred via vehicular mechanism. The conductivities of the MF-4SK, CM-1 and CMX membranes depend very slightly on the equilibrium solution concentrations, while the conductivity of membrane MK-40 rises with the increasing concentration of both NaCl and HCl. As is well known from other investigations [51,53], the structure of membrane MK-40 is heterogeneous, and the volume fraction of the 'inter-gel' phase is around 0.2. In accordance with the microheterogeneous two-phase model, the membrane's heterogeneity leads to a pronounced dependence of the membrane conductivity on the concentration of equilibrium electrolyte solution. In NaCl solutions, membrane MK-40 has the lowest conductivity in the concentration range 0–0.25 M, whereas from 0.25 to 0.50 M its conductivity is comparable to that of CMX and MF-4SK. Compared to the other three membranes, membrane CM-1 possesses the highest conductivity in the investigated range of NaCl concentration. Comparison of the membrane conductivities in HCl solutions (Fig. 4b) showed that membrane CMX has almost the lowest conductivity of the entire investigated concentration range (from 0.05 to 0.50 M). MF-4SK and CMX exhibit practically the same conductivity in HCl solutions. The conductivity of MK-40 is lowest in the range of 0–0.04 M HCl, but around 0.05 M it is equal to that of CMX, and at 0.10 M it is comparable to CM-1 and MF-4SK. From 0.10 to 0.50 M HCl membrane MK-40 has the highest conductivity of all of the investigated membranes.

Fig. 5 presents the concentration dependencies of the specific membrane conductivity in bi-logarithmic coordinates lg κ_m–lg κ_{sol}.

Table 2
Physico-chemical characteristics and model parameters of the membranes.

Membrane	W (% g/g$_{dry}$)	Q (mmol/g$_{swol}$)	d_m (g/cm^3)[a]	$\overline{\kappa} \times 10^3$, (S/cm)	f_1	f_2
NaCl						
MF-4SK	13.54	0.82	1.67	7.04	0.96	0.04
MK-40	50.30	1.69	1.13	5.27	0.82	0.18
CM-1	37.50	1.56	1.18	9.19	0.95	0.05
CMX	27.5	1.29	1.19	6.72	0.94	0.06
HCl						
MF-4SK	18.88	0.78	1.53	34.63	0.96	0.04
MK-40	58.30	1.60	1.10	34.02	0.80	0.20
CM-1	40.25	1.53	1.13	34.68	0.96	0.04
CMX	32.22	1.25	1.13	30.92	0.96	0.04

[a] The density was measured for water-swollen membranes.

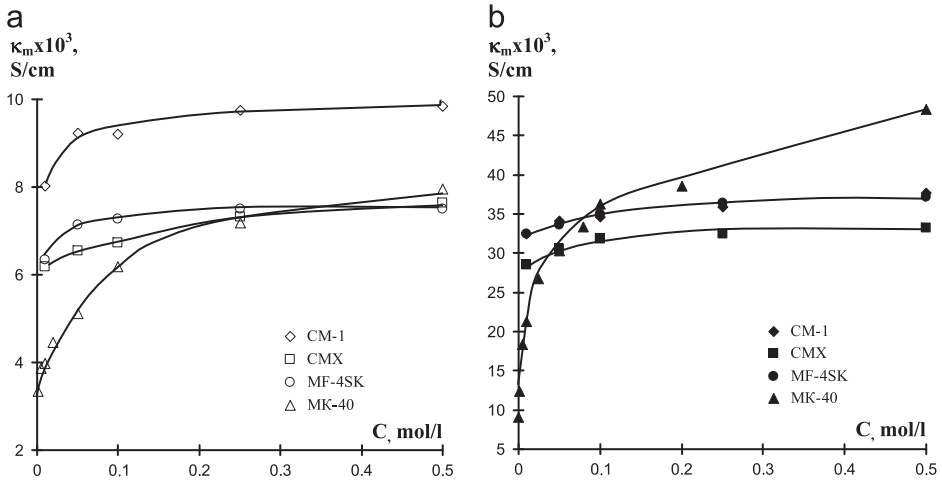

Fig. 4. Concentration dependencies of the membrane specific conductivity in (a) NaCl and (b) HCl solutions.

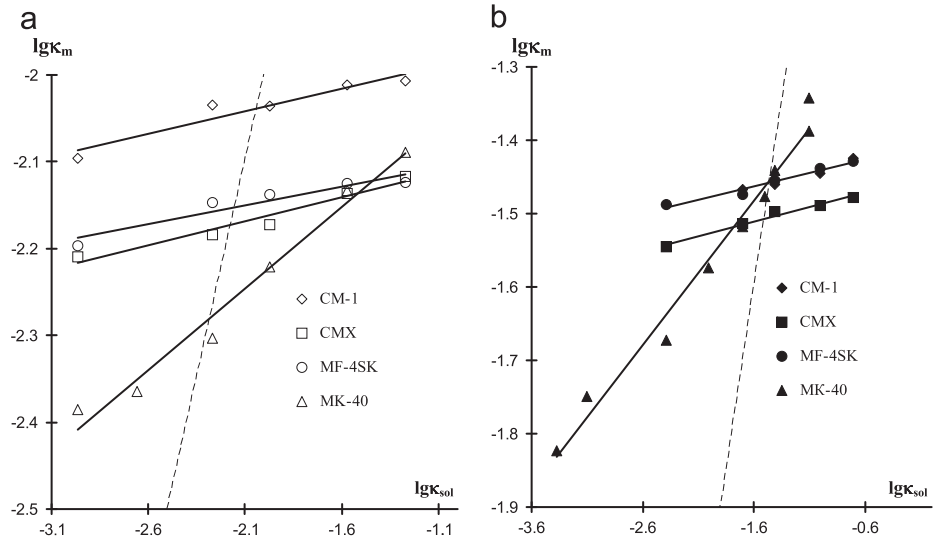

Fig. 5. Concentration dependencies of the membrane conductivity in bi-logarithmic coordinates: (a) NaCl and (b) HCl. The dotted line specifies the linear relation $\lg\kappa_m = \lg\kappa_{sol}$ used to determine the membrane conductivity in the iso-conductance point.

Based on the approach of the microheterogeneous model, the volume fraction of the 'inter-gel' phase (f_2) has been found from the slope of the linear fit $\lg\kappa_m = a \cdot \lg\kappa_{sol} + b$. The iso-conductance point ($\bar{\kappa}$) has been determined from the point of intersection with $\lg\kappa_m = \lg\kappa_{sol}$. The calculated structural parameters f_1, f_2 and $\bar{\kappa}$ for the investigated membranes are presented in Table 2. As seen from the data, membrane MK-40 has the highest degree of heterogeneity with a parameter f_2 of around 0.20. This corresponds well with other researches [49–51]. The values of the 'gel' phase volume fraction for CM-1 and MF-4SK are close to those found for the CM-2 membrane (with close properties to CM-1) and Nafion 117 (which is very similar to MF-4SK) by Chaabane. et al. [52]. According to the membrane classification [53], and based on the volume fraction of the 'inter-gel' phase f_2, membranes MF-4SK, CM-1 and CMX can be referred to as homogeneous because $0 < f_2 < 0.15$, whereas membrane MK-40 is heterogeneous with $0.15 < f_2 < 0.30$.

From the data given in Table 2, the following transport characteristics of the counter-ions H^+ and Na^+ in the membrane 'gel' phase were calculated: the hydration capacity of the 'gel' phase $\overline{n}$ (Eq. (7)), the counter-ion diffusion coefficient $\overline{D}$ (Eq. (5)), and the molar conductivity $\overline{\lambda}$ (Eq. (6)). In Fig. 6 the diffusion coefficient $\overline{D}$ and the molar conductivity $\overline{\lambda}$ of H^+ and Na^+ are plotted as a function of the hydration capacity of the 'gel' phase $\overline{n}$. For all four membranes the hydration capacities of the membrane 'gel' phases in H^+-forms is larger than in Na^+-forms. The counter-ions transport characteristics ($\overline{\lambda}$,$\overline{D}$) in the following ways: MK-40 < CM-1 < CMX < MF-4SK and MK-40 < CMX < CM-1 < MF-4SK in proton and sodium forms, respectively. Membrane MK-40 has the lowest hydration capacity and molar conductivity in both Na^+ and H^+-forms. The highest molar conductivity and diffusion coefficient of Na^+ is observed in membrane MF-4SK, although the hydration capacity of the perfluorosulfonated membrane is lower than that of membranes CM-1 and CMX. In H^+-form the membrane MF-4SK possesses the highest hydration capacity, as well as the highest molar conductivity and diffusion coefficient. In this paper the diffusion coefficient of the proton calculated for the 'gel' phase of MF-4SK is 7.75×10^{-6} cm^2/s. Our calculated proton diffusion coefficient corresponds well with other experimental and computational studies: Karo et al. [22] carried out the classical molecular modeling of Nafion with an effective hydration level of 15 at 363 K, and obtained 6.15×10^{-6} cm^2/s; Perrin et al. [61] measured the vehicular proton transport using the quasi-elastic

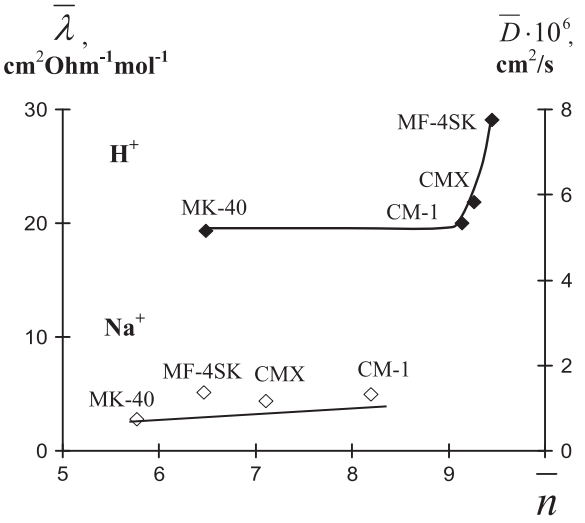

Fig. 6. Transport characteristics $\overline{\lambda}$, $\overline{D}$ of counter-ions Na^+ and H^+ in the membrane 'gel' phase vs. specific hydration capacity of the 'gel' phase $\overline{n}$.

Table 3
Relation of the limiting molar conductivity of H^+, Na^+ to the molar conductivity in membrane 'gel' phase.

Membrane	$\lambda_\infty/\overline{\lambda}$	
	Na^+	H^+
MF-4SK	9.78	12.02
MK-40	18.22	18.12
CM-1	10.08	17.44
CMX	11.53	15.99

λ_∞ (Na^+)=50.28 $cm^2\ \Omega^{-1}\ mol^{-1}$ [62].
λ_∞ (H^+)=349.80 $cm^2\ \Omega^{-1}\ mol^{-1}$[62].

neutron and scattering method, and obtained a diffusion coefficient of 4×10^{-6} cm^2/s.

Table 3 displays the ratio of the limiting molar conductivity (λ_∞) of the proton and sodium ion in water [62] compared to the molar conductivity in the membrane 'gel' phase ($\overline{\lambda}$). This ratio $\lambda_\infty/\overline{\lambda}$ describes the molar conductivity of the proton during transfer from water to the membrane 'gel'′ phase, which with a value above 18 was the highest for MK-40, as well as for both ionic-forms. The lowest ratio was observed for membrane MF-4SK, with a value of 12 in H^+-form and around 10 in Na^+-form. As seen from the data, among these four investigated membranes the proton and sodium ions possess the largest molar conductivity and diffusion coefficient in the 'gel' phase of the perfluorosulfonated membrane MF-4SK. The computational investigations of the two membrane types MK-40 and MF-4SK were carried out in order to better understand the influence of the polymer structural features on the transport characteristics of counter-ions.

5.2. Computational results

In this section the theoretical results are discussed in regard to the correlation between the chemical structure, including the water state, and the membrane conductivity. Quantum chemical investigations were carried out at various hydration levels (X) with models of the membranes MK-40 and MF-4SK. The investigation for the MK-40 membrane was carried out in Na^+ and H^+-forms from 0 up to 8, and for MF-4SK from 0 up to 8 in Na^+-form and up to 10 in H^+-form. The optimized structures of the membrane models are shown in the dry state for both membranes, with one, three, six and eight water molecules in Na^+-form in Fig. 7, and in H^+-form in Fig. 8. The geometry parameters of the dry membranes and the membranes containing three water molecules are presented in Tables 4 and 5.

The comparison of the geometries of the dry MF-4SK and MK-40 membranes in H^+-form shows that the average S…O distances of the $-SO_3^-$ group are slightly larger in the aromatic membrane MK-40 (average 1.48 Å) than in the perfluorinated membrane MF-4SK (average 1.46 Å), while the distance C(1)–S is shorter in the membrane MK-40 (1.76 Å) than in the membrane MF-4SK (1.84 Å).

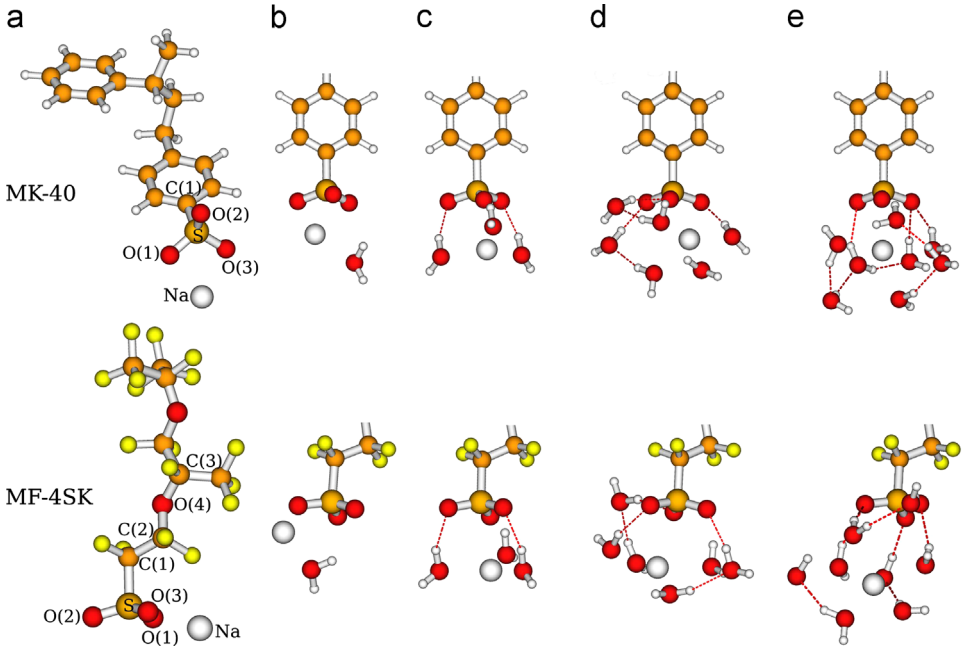

Fig. 7. Calculated geometries of dry membranes (a) and membrane fragments (b–e) in Na^+-form at various hydration levels: X=1 (b); X=3 (c); X=6 (d); X=8 (e) for MK-40 (top) and MF-4SK (bottom).

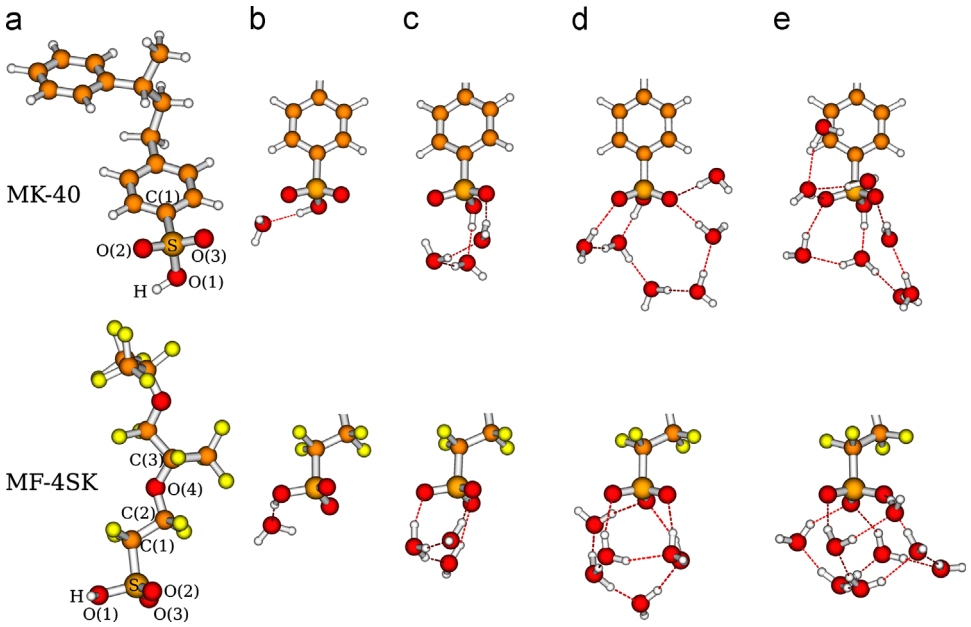

Fig. 8. Calculated geometries of dry membranes (a) and hydrated membrane fragments (b–e) in H^+-form at various hydration levels: $X=1$ (b); $X=3$ (c); $X=6$ (d); $X=8$ (e) for MK-40 (top) and MF-4SK (bottom).

Table 4
Geometry parameters of MF-4SK membrane in H^+ and Na^+ forms for the dry state and with three water molecules per sulfo group.

Parameter	Atom/Group	H^+-form		Na^+-form	
		MF-4SK	MF-4SK · $3H_2O$	MF-4SK	MF-4SK · $3H_2O$
Bond length (Å)	C(1)–F	1.326	1.325	1.325	1.328
		1.318	1.325	1.325	1.326
	S–O(1,2,3)	1.409	1.442	1.420	1.443
		1.417	1.465	1.462	1.457
		1.565	1.442	1.460	1.441
	C(1)–S	1.835	1.830	1.837	1.831
	O(1)–H^+/Na^+	0.952	1.557	2.268	O(1)–Na 3.651
				2.245	O(2)–Na 3.640
					O(3)–Na 2.360
	S..H^+/Na^+	2.112	2.578	2.768	3.245
Angle (deg)	C(1)–S..H^+/Na^+	98.9	134.6	108.5	143.8
	C(1)–S–O(1)–H^+/Na^+	−93.1	179.8	−103.30	C(1)–S–O(3)–Na–178.4
	S–C(1)–C(2)–O(4)	175.5	176.5	163.1	175.7
	C(1)–C(2)–O(4)–C(3)	153.9	154.5	154.4	154.7

Table 5
Geometry parameters of MK-40 membrane in H^+ and Na^+ forms for the dry state and with three water molecules per sulfo group.

Parameter	Atom/Group	H^+-form		Na^+-form	
		MK-40	MK-40 · $3H_2O$	MK-40	MK-40 · $3H_2O$
Bond length (Å)	S–O(1,2,3)	1.420	1.434	1.435	1.455
		1.429	1.437	1.477	1.456
		1.587	1.554	1.477	1.472
	C(1)–S	1.759	1.755	1.773	1.769
	O(1)–H^+/Na^+	0.949	0.977	2.219	2.301
				2.216	
	S..H^+/Na^+	2.114	2.133	2.744	3.229
Angle (deg)	C(1)–S..H^+/Na^+	106.8	125.7	122.6	146.9
	C(1)–S–O(1)–H^+/Na^+	−101.2	−171.6	119.0	−179.4

In the hydrated state with three water molecules, the acidic group $-SO_3H$ dissociates and the average S…O distance of MF-4SK becomes shorter (1.45 Å) in comparison to the dry state.

Fig. 9 demonstrates the distances between the nearest oxygen atom of the $-SO_3^-$ group and the proton or counter-ion respectively, as a function of the membrane hydration level. In the perfluorinated membrane MF-4SK, both of the counter-ions (H^+, Na^+) are removed from the $-SO_3^-$ group with the increasing hydration level, while in the aromatic membrane MK-40, both of the counter-ions remain bound to the $-SO_3^-$ group with an almost invariant SO…Na^+/H^+ distance. This can also be seen well in Figs. 7 and 8. The sodium ion in membrane MK-40 is sitting close

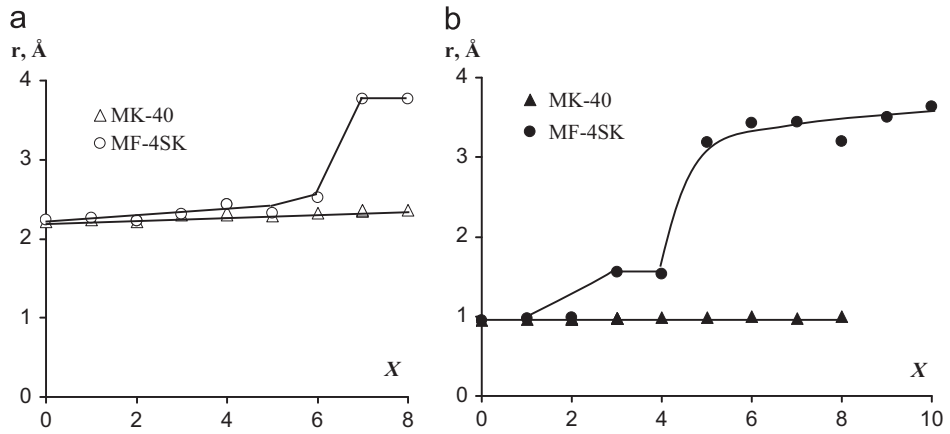

Fig. 9. Oxygen-counter-ion distance $–SO_3^-…Na^+$ (a) and $–SO_3^-…H^+$ (b) in membranes MF-4SK and MK-40 as a function of the hydration level.

to the $–SO_3^-$ group throughout the entire investigated range of the hydration level $X=0–8$ with a distance of Na…O of 2.22–2.37 Å (Figs. 7 and 9a). The Na…O distance in MF-4SK increases very slightly from 2.25 to 2.52 Å with the increase in hydration level from 0 up to 6, and rises sharply at $X=7$, reaching 3.77 Å, because the sodium ion moves from the first to the second solvation shell. As seen in Fig. 9, the $–SO_3^-…H^+$ distance in membrane MK-40 stays practically invariant throughout the entire investigated range of the hydration level. In MF-4SK, this distance changes from 0.95 to 0.99 Å at $X=0–2$. The first sharp rise of the $–SO_3^-…H^+$ distance to 1.56 Å occurs at $X=3$, when the proton builds the hydronium ion with the neighboring water molecule. The second pronounced increase of this distance to 3.19 Å is observed at $X=5$, when the hydronium ion transfers from the first to the second solvation shell.

Although one cannot reach conclusions about the transport behavior of counter-ions from static geometry calculations, we assume that the larger distance between the counter-ion and sulfo- group in MF-4SK compared to MK-40 might be one of the reasons why the sodium ion and proton in MF-4SK have a somewhat higher mobility, and therefore larger molar conductivity than in MK-40 (as seen from Fig. 6). In contrast to the sodium ion, the proton is able to hop via the Grotthuss mechanism, which explains the larger conductivity of the protonated form of membrane compared to the sodium ion form. Recent studies on Nafion using the self-consistent multistate empirical valence bond method [31] demonstrated that the proton hopping mechanism dominates at higher hydration levels. The quantum mechanical geometries confirm these findings in our static picture: by adding 3 water molecules to the H^+-form of the membranes, a network of waters including the interaction with the $–SO_3^-$ group was formed as the most stable conformation (see Fig. 8c). At higher hydration levels this stable water cluster below the $–SO_3^-$ group enlarges to form a dense water network, and the proton moves farther away from the $–SO_3^-$ group to the second solvation shell. This latter fact can be interpreted as a sufficient condition for a fast proton hopping mechanism. In a dynamic process this results in a higher probability of interaction with neighboring water or sulfonate ions, and leads to higher mobility. In contrast to the H^+ form, the Na^+ form of both membrane models does not show such a water cluster at hydration level $X=3$, and the water network is sparser.

In the H^+-form, the greatest difference between the two membrane types is the dissociation of the $–SO_3H$ group in the perfluorinated membrane MF-4SK at the hydration level $X\geq3$, in contrast to the polystyrene membrane MK-40 (Fig. 8). With the inclusion of three water molecules, two topologically different conformations of the MF-4SK model could be located in our calculations: one in the dissociated $–SO_3^-…H^+$ group, and a second one in the undissociated $–SO_3H$group. The undissociated conformation has a high relative energy of 3.58 kJ/mol and 15.27 kJ/mol, calculated by the RHF/6–31+G(d,p) and LPNO-CEPA/def2-TZVP methods respectively. This confirms the strong acidity of the $–SO_3H$ group.

This dissociation behavior of the functional group in the ion-exchange membranes has been investigated intensively by different computational methods. Since the side chain of the membrane MF-4SK has a structure similar to Nafion, our computational results can be directly compared to studies on Nafion. For the Nafion side chain, as well as for shorter perfluorinated chains, the dissociation of the $–SO_3H$ group with more than three water molecules is well known in accordance with quantum chemical calculations and MD simulations [15–18,20–22]. During their studies of the shorter Dow side chain with up to seven or nine water molecules, Paddison et al. [20] detected that the dissociation occurs at a solvation level higher than six for two side chains or three for one chain. Other quantum mechanical studies [13,17] and MD simulations [21,22] on Nafion side chains confirm that the dissociation takes place at hydration level $X=3$. Devanathan et al. [18] performed MD studies of neutral Nafion clusters with 4 and 8–48 chains at hydration levels $X=5–15$, and established the migration of H_3O^+ outside of the first solvation shell of the sulfonic acid group. At the hydration level of between 5 and 6 water molecules per sulfo- group, they discovered that the hydrated functional groups build a continuous cluster phase where the proton can move without barriers. At this level of hydration Nafion membranes begin to conduct electrical current, and it is considered to be the percolation threshold. Malek et al. [63] detected water percolation at $X=4$ in their simulations of Nafion with the hydration levels $X=2, 4, 9, 15$.

In contrast to the perfluorinated membranes, the investigated aromatic membranes do not show the dissociation of the $–SO_3H$ group in water. Idupulapati [13] describes aromatic membranes using the quantum mechanical RHF and DFT methods. These demonstrate that the sulfo groups in aromatic membranes based on SPEEK do not dissociate at the hydration level of up to six water molecules. This is in agreement with our findings for the aromatic MK-40 membrane model.

The binding energy of water is another characteristic property which defines the thermodynamic state of the water around the sulfo groups in membranes. The binding energies of the membrane-water clusters were calculated by Eq. (2). Fig. 10 graphically depicts the LPNO-CEPA binding energies per water molecule for all four membrane models. It demonstrates that the water molecules in the Na^+-form of both the MF-4SK and MK-40 membranes are more strongly bound than in the H^+-form of these

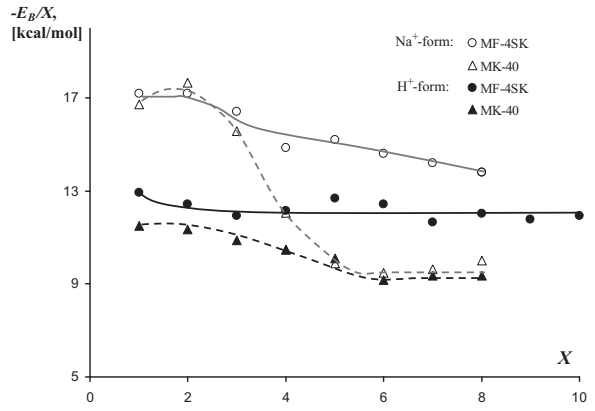

Fig. 10. Binding energy per water vs. number of absorbed water molecules (X) in membranes MK-40 and MF-4SK in Na^+ and H^+-forms.

membranes. Therefore we can assume that the diffusion coefficient of the water molecules must be higher in the H^+-form of the membranes than in the Na^+-form. This assumption was confirmed by the values of the self-diffusion coefficients in membrane MF-4SK obtained by Volkov et al. [64] using NMR-measurements.

Comparison of the water network around the $-SO_3^-$ group in the Na^+-form of the membranes shows that the water molecules in MF-4SK are more strongly connected than in MK-40. In the Na^+-form of both membranes the binding energy of the first three water molecules does not differ significantly. However, at the higher hydration level $X > 4$ the water is more strongly bound in MF-4SK than in MK-40. For MK-40 both forms are converging to the same value 9.5 kcal/mol.

In the H^+-form, the perfluorosulfonated membrane MF-4SK has a higher water binding energy than the aromatic membrane MK-40, consisting of approximately 2 kcal/mol at the higher hydration level $X \geq 6$. From these results we can conclude that the water molecules are more strongly bound in the H^+-form of MF-4SK than in MK-40, and that the water is more strongly connected in the perfluorinated membrane than in the polystyrene membrane. This results in a higher mobility of the protons in the perfluorinated membrane relative to the aromatic membrane.

As shown in the Figs. 7e and 8e for high hydration level, for both ionic forms the eight water molecules build a stronger network below the $-SO_3^-$ group in MF-4SK than in MK-40. In particular, the H^+-form of the aromatic membrane MK-40 shows an expanded distribution of the water molecules. This is also reflected in the OH…O hydrogen bond distances between the water molecules. MF-4SK has an average hydrogen bond distance of 1.85 Å in its H^+-form, and a longer distance of 2.03 Å in its Na^+-form. The latter is in the same range as MK-40, which is 2.02 Å in both forms.

It is well known that water itself predominantly forms clusters of 6 water molecules in a ring-like structure. Kim J. and Kim K.S. computed the binding energy of water in such a hexa-water cluster using the MP2 method with 30 kcal/mol [65], and Bryantisev et al. received MP2-CBS values of 45.6–45.9 kcal/mol for four different conformations of hexa-water clusters [66], that corresponds to 7.6–7.7 kcal/mol binding energy per one water molecule. Our LPNO-CEPA calculations of the H^+-form of the perfluorinated membrane MF-4SK at hydration level $X > 6$ converge to a value of 12.2 kcal/mol and to 9.5 kcal/mol for MK-40 membrane, as shown in Fig. 10. This fact confirms numerous experimental investigations showed that the water molecules in the ion-exchange membranes are stronger bound than in the bulk water [45–48].

The results obtained show that the chemical nature of the membrane polymer matrix has some influence on the dissociation of the functional groups, as well as on the building of the water cluster in the ion-exchange membranes. The dissociation of $-SO_3^-...H^+$ observed in the perfluorinated membrane and well-networked water molecules can promote the improved transport of the protons by the Grotthuss mechanism. These results explain the experimental investigations, which indicate higher proton mobility in the perfluorinated membranes compared to the polystyrene membranes.

6. Conclusion

In this paper the physico-chemical characteristics (density, water uptake, ion-exchange capacity) and concentration dependencies of four commercial cation-exchange membranes (MF-4SK, MK-40, CM-1, CMX) were investigated experimentally in HCl and NaCl aqueous solutions. The water uptake of all four membranes is higher in Na^+-form than in H^+-form, while the ion-exchange capacity and density of the membranes in Na^+-form are lower than in H^+-form. Using the approaches of the microheterogeneous two-phase model for ion-exchange membrane conductivity, the volume fractions of the 'gel' and 'inter-gel' phases, as well as the hydration capacity and conductivity of the 'gel' phase were estimated from the measured concentration dependencies of the membrane conductivity. The volume fraction of the 'gel' phase f_2 in membranes MF-4SK, CM-1 and CMX is around 0.04–0.06. Therefore the membranes can be considered to be homogeneous. Because parameter f_2 of MK-40 is 0.18–0.20, this membrane is rated as heterogeneous. The conductivity of the 'gel' phase of the membranes changes in the following sequence: for Na^+-form MK-40 < CMX < MF-4SK < CM-1; for H^+-form CMX < MK-40 < MF-4SK < CMX. In order to analyze the transport properties of the counter-ions, the molar conductivity $\overline{\lambda}$ and diffusion coefficient $\overline{D}$ were calculated from the obtained experimental data and based on the model structural parameters of the membranes. In comparison to the other membranes investigated, H^+ and Na^+ possess the highest $\overline{\lambda}$ and $\overline{D}$ in the perfluorinated membrane MF-4SK. The transport characteristics ($\overline{\lambda}$, $\overline{D}$) of the counter-ions in the membrane 'gel' phase follow the sequences: for Na^+ MK-40 < CM-X < CM-1 < MF-4SK; for H^+ MK-40 < CM-1 < CMX < MF-4SK. The calculated diffusion coefficient $\overline{D}$ of the proton in the perfluorinated membrane (7.75×10^{-6} cm^2/s) corresponds to the quantity calculated using the molecular dynamics method [22], and obtained through experimental measurements [61].

Using ab-initio quantum chemical methods, the structures and water binding energies of the aromatic membrane MK-40, having a hydrocarbon polymer-backbone, and of the non-aromatic membrane MF-4SK, having a tetrafluoroethylene polymer matrix, were calculated at various hydration levels of these membrane models. In the perfluorinated membrane MF-4SK, the dissociation of the $-SO_3H$ group is observed at the hydration level $X \geq 3$, while no dissociation is observed in the aromatic poly-styrene membrane MK-40.

In the membrane MF-4SK, the distance $-SO_3^-...H^+$ grows dramatically during the first step of H^+ dissociation at $X = 3$, as well as during the second step at $X > 5$, when the proton moves to the second solvation shell. The increasing $-SO_3^-...Na^+$ distance in MF-4SK was detected at $X > 5$, however with a weaker water network than the proton form. In the aromatic membrane MK-40, the distance between the counter-ion and the $-SO_3^-$ group practically does not change along the entire investigated range of the membrane hydration level ($0 \leq X \leq 8$) in both H^+ and Na^+-forms.

The binding energy of the water in the Na^+-form is higher than in the H^+-form, which represents a stronger binding of the water molecule. In addition, the water molecules around the $-SO_3^-$ group in the H^+-form of MF-4SK show a stronger network than in the aromatic membrane MK-40.

The observed dissociation of the functional groups in the perfluorinated membrane MF-4SK, as well as the stronger water network explain the higher $\overline{\lambda}$ and $\overline{D}$ of Na^+ and H^+ in comparison to the other membranes investigated in this paper.

References

[1] M. Mulder, Basic Principles of Membrane Technology, Klumer Academic Publishers, 1996.
[2] H. Strathmann, Ion-exchange membrane separation processes (Membrane Science and Technology Series), Elsevier Ltd., 2004.
[3] S.J. Peighambardoust, S. Rowshanzamir, M. Amjadi, Review of the proton exchange membranes for fuel cell applications, Int. J. Hydrogen Energy 35 (17) (2010) 9349–9384.
[4] Y. Wang, K.S. Chen, J. Mishler, S.C. Cho, X.C. Adroher, A review of polymer electrolyte membrane fuel cells: technology, applications, and needs on fundamental research, Appl. Energy 88 (2011) 981–1007.
[5] J. Luo, C. Wu, T. Xu, Y. Wu, Diffusion dialysis-concept, principle and applications, J. Membr. Sci. 366 (2011) 1–16.
[6] S. Koter, Ion-exchange membranes for electrodialysis - A patents review, Recent Pat. Chem. Eng. 4 (2) (2011) 141–160.
[7] R. Devanathan, Recent developments in proton exchange membranes for fuel cells, Energy Environ. Sci. 1 (2008) 101–119.
[8] S. Koter, P. Piotrowski, J. Kerres, Comparative investigation of ion-exchange membranes, J. Membr.Sci. 153 (1999) 83–90.
[9] M. Saito, A Naoko, H Kikuko, T Okada, Mechanisms of ion and water transport in perfluorosulfonated ionomer membranes for fuel cells, J. Phys. Chem. B. 108 (2004) 16064–16070.
[10] D. Brandell, J. Karo, A. Liivat, J.O. Thomas, Molecular dynamics studies of the Nafion, Dow and Aciplex fuel-cell polymer membrane systems, J. Mol. Model 13 (2007) 1039–1046.
[11] E. Kim, P.E. Weck, N. Balakrishnan, C. Bae, Nanoscale building blocks for the development of novel proton exchange membrane fuel cells, J. Phys. Chem. B. 112 (2008) 3283–3286.
[12] C.V. Mahajan, V. Ganesan, Atomistic simulations of structure of solvated sulfonated poly(ether ether ketone) membranes and their comparisons to nafion: I. nanophase segregation and hydrophilic Domains, J. Phys. Chem. B 114 (2010) 8357–8366.
[13] N. Idupulapati, R. Devanathan, M. Dupuis, Ab initio study of hydration and proton dissociation in ionomer membranes, J. Phys. Chem. A. 114 (2010) 6904–6912.
[14] M. Tsuda, H. Kasai, Solvent effects on anionic and acid forms of nafion side chain, Jap. J. Appl. Phys 45 (6A) (2006) 5121–5125.
[15] E. Spohr, P. Commer, A.A. Kornyshev, Enhancing proton mobility in polymer electrolyte membranes: lessons from molecular dynamics simulations, J. Phys. Chem. B. 106 (2002) 10560–10569.
[16] S.J. Paddison, J.A. Elliott, Molecular modeling of the short-side-chain perfluorosulfonic acid membrane, J. Phys. Chem. A. 109 (2005) 7583–7593.
[17] S.J. Paddison, J.A. Elliott, Selective hydration of the 'short-side-chain' perfluorosulfonic acid membrane. An ONIOM study, Solid State Ionics 178 (2007) 561–567.
[18] R. Devanathan, R Venkatnathan, R. Rousseau, M. Dupuis, T. Frigato, W. Gu, V. Helms, Atomistic simulation of water percolation and proton hopping in Nafion fuel cell membrane, J. Phys. Chem. B. 114 (2010) 13681–13690.
[19] N.P. Berezina, L.V. Karpenko, O.A. Dyomina, Yu.E. Kirsh, E.N. Komkova, Dependence of the electrotransport properties of polyarylene sulfamide membranes on their chemical composition and concentration of equilibrium electrolyte solutions, Rus. J. Electrochem. 33 (5) (1997) 550–555.
[20] S.J. Paddison, T.A. Zawodzinski Jr., Molecular modeling of the pendant chain in Nafion, Solid State Ionics 113–115 (1998) 333–340.
[21] E. Spohr, Molecular dynamics simulations of proton transfer in a model Nafion pore, Mol. Simulation 2–3 (30) (2004) 107–115.
[22] J. Karo, A. Aabloo, J.O. Thomas, D. Brandell, Molecular dynamics modeling of proton transport in nafion and hyflon nanostructures, J. Phys. Chem. B. 114 (18) (2010) 6056–6064.
[23] V.I. Volkov, E.V. Volkov, S.V. Timofeev, E.A. Sanginov, A.A. Pavlov, E. Yu. Safronova, I.A. Stenina, Water self-diffusion and ionic conductivity in perfluorinated sulfocationic membranes MF-4SK, Rus. J. Inorg. Chem. 55 (3) (2010) 315–317.
[24] N.P. Berezina, N.A. Kononenko, O.A. Dyomina, N.P. Gnusin, Characterization of ion-exchange membrane materials: Properties vs structure, Adv. Colloid Interface Sci. 139 (2008) 3–28.
[25] J.K. Clark, S.J. Paddison, M. Eikerling, M. Dupuis, T.A. Zawodzinski, A comparative ab initio study of the primary hydration and proton dissociation of various imide and sulfonic acid ionomers, J. Phys. Chem. A. 116 (7) (2012) 1801–1813.
[26] D.W. Hofmann, L. Kuleshova, B.D. Di Noto, E. Negro, F. Conti, M. Vittadello, Investigation of water structure in Nafion membranes by infrared spectroscopy and molecular dynamics simulation, J. Phys. Chem. B. 113 (2009) 632–639.
[27] V.A. Shaposhnik, E.V. Butyrskaya, Computer simulation of cation-exchange membrane structure: An elementary act of hydrated ion transport, Rus. J. Electrochem. 40 (7) (2004) 767–770.
[28] S. Urata, J. Irisawa, A. Takada, W. Shinoda, S. Tsuzuki, M. Mikami, Molecular dynamics simulation of swollen membrane of perfluorinated ionomer, J. Phys. Chem. B. 109 (2005) 4269–4278.
[29] J. Liu, N. Suraweera, D.J. Keffer, S. Cui, S.J. Paddison, On the relationship between polymer electrolyte structure and hydrated morphology of perfluorosulfonic acid membranes, J. Phys. Chem. C. 114 (2010) 11279–11292.
[30] M.E. Selvan, D.J. Keffer, S. Cui, S.J. Paddison., A reactive molecular dynamics algorithm for proton transport in aqueous systems, J. Phys. Chem. C. 114 (2010) 11965–11976.
[31] S. Feng, G.A. Voth, Proton solvation and transport in hydrated Nafion, J. Phys. Chem. B 115 (2011) 5903–5912.
[32] DuPontTM Nafion® PFSA Membranes. Data Sheet (DuPont Fuel Cells). 2010.
[33] GOST 17552-72; GOST 17553-72; GOST 17554-72 (State Standard, Russia).
[34] L.V. Karpenko, Electro-transport properties of the ion-exchange membranes as a function of the polymer composition and the concentration of the equilibrium electrolyte solution, Ph.D. thesis, Kuban State University Krasnodar, Russia 1999(in Russian).
[35] L.V. Karpenko, O.A Dyomina, G.A Dvorkina, S.B. Parshikov, Cr Larchet, B. Auclair, N.P. Berezina, Comparative study of methods used for the determination of electroconductivity of ion-exchange membranes, Rus. J. Electrochem. 3 (2001) 328–335.
[36] A.I. Meshechkov, O.A. Demina, N.P. Gnusin, Impedance diagram of a mercury-contact cell with ion-exchange membrane, Sov. Electrochem. 23 (10) (1988) 1364–1367.
[37] W.J. Hehre, R Ditchfield, J.A Pople, Self-consistent molecular orbital methods. XII. Further extensions of gaussian-type basis sets for use in molecular orbital studies of organic molecules, J. Chem. Phys 56 (1972) 2257–2261.
[38] C. Wang, J.K. Clark II, M. Kumar, S.J. Paddison, An ab initio study of the primary hydration and proton transfer of CF_3SO_3H and $CF_3O(CF_2)_2SO_3H$: Effects of the hybrid functional and inclusion of diffuse functions, Solid State Ionics 199–200 (2011) 6–13.
[39] F. Weigend, R Ahlrichs, Balanced basis sets of split valence, triple zeta valence and quadruple zeta valence quality for H to Rn: Design and assessment of accuracy, PCCP 7 (2005) 3297–3305.
[40] F. Neese, F. Wennmohs, A. Hansen, Efficient and accurate local approximations to coupled-electron pair approaches: An attempt to revive the pair natural orbital method, J. Chem. Phys 130 (2009), art. no. 114108.
[41] Neese, F. ORCA Version 28., An ab initio, density functional and semiempirical program package; University Bonn, Sept. 2010.
[42] N.P. Gnusin, V.I. Zabolotzki, V.V. Nikonenko, A.I. Meshechkov, Development of the principle of the generalize conductivity to describe transport phenomena in disperse systems caused by the different driving forces, Zh. Fiz. Khim 54 (1980) 1518–1522.
[43] V.I. Zabolotsky, V.V. Nikonenko, Effect of structural membrane inhomogeneity on transport properties, J. Membr. Sci. 79 (1993) 181–198.
[44] C. Larchet, S. Nouri, B. Auclair, L. Dammak, V. Nikonenko, Application of chronopotentiometry to determine the thickness of diffusion layer adjacent to an ion-exchange membrane under natural convection, Adv. Colloid Interface Sci. 139 (2008) 45–61.
[45] H.R. Corti, F. Nores-Pondal, B.M. Pilar, Low temperature thermal properties of Nafion 117 membranes in water and methanol-–water mixtures, J. Power Sources 161 (2006) 799–805.
[46] M. Iijima, Y. Sasaki, T. Osada, K. Miyamoto, M. Nagai, Nanostructure of clusters in nafion studied by DSC, Int. J. Thermophysics 27 (6) (2006) 1792–1802.
[47] S.J. Lue, S.-J. Shieh, Water states in perfluorosulfonic acid membranes using differential scanning calorimetry, J. Macromol. Sci. Phys. 48 (2009) 114–127.
[48] M.T. Brik, V.I. Zabolotsky, I.D. Atamanenko, G.A. Dvorkina, Structural heterogeneity of ion-exchange membranes in swollen state and methods to study, Khimiya i Tekhnologiya Vodyi (in Russian) 11 (6) (1989) 491–497.
[49] V.P. Beketova, Influence of the structural heterogeneity on the transport properties of the ion-exchange membranes, Ph.d. thesis, Krasnodar, Russia, 1977(in Russian).
[50] C. Larchet, L. Dammak, B. Auclair, S. Parchikov, V. Nikonenko, A simplified procedure for ion-exchange membrane characterisation, New J. Chem. 28 (2004) 1260–1267.
[51] N. Berezina, N. Gnusin, O. Dyomina, S Timofeyev, Water electrotransport in membrane systems Experiment and model description, J. Membr. Sci. 86 (1994) 204–229.
[52] L. Chaabane, L. Dammaka, V.V. Nikonenko, G. Bulvestre, B. Auclair., The influence of absorbed methanol on the conductivity and on the microstructure of ion-exchange membranes, J. Membr. Sci. 298 (2007) 126–135.
[53] N.P. Gnusin, N.P. Berezina, O.A. Dyomina, N.A. Kononenko, Physicochemical principles of testing ion-exchange membranes, Rus, J. Electrochem. 32 (2) (1996) 154–163.
[54] A. Elattar, A. Elmidaoui, N. Pismenskaia, C. Gavach, G. Pourcelly, Comparison of transport properties of monovalent anions through anion-exchange membranes, J. Membr. Sci. 143 (1998) 249–261.
[55] J.H. Choi, S.H. Kim, S.H. Moon, Heterogeneity of ion-exchange membranes: the effects of membrane heterogeneity on transport properties, J. Colloid Interface Sci. 241 (2001) 120–126.

[56] N.P. Gnusin, N.P. Berezina, N.A. Kononenko, O.A. Dyomina, Transport structural parameters to characterize ion exchange membranes, J. Membr. Sci. 243 (2004) 301–310.
[57] X.T Le, Permselectivity and microstructure of anion exchange membranes, J. Colloid Interface Sci. 325 (2008) 215–222.
[58] N.P. Berezina, A-A. Kubaisy, S.V. Timofeev, L.V. Karpenko, Template synthesis and electrotransport behavior of polymer composites based on perfluorinated membranes incorporating polyaniline, J. Solid State Electrochem. 11 (2007) 378–389.
[59] L.V. Karpenko-Jereb, N.P. Berezina, Determination of structural, selective, electrokinetic and percolation characteristics of ion-exchange membranes from conductive data, Desalination 245 (2009) 587–596.
[60] N.P. Berezina, S.V. Timofeev, N.A. Kononenko, Effect of conditioning techniques of perfluorinated sulphocationic membranes on their hydrophylic and electrotransport properties, J. Membr. Sci. 209 (2) (2002) 509–518.
[61] J-C. Perrin, S. Lyonnard, F. Volino, Quasielastic neutron scattering study of water dynamics in hydrated Nafion membranes, J. Phys. Chem. C. 111 (2007) 3393–3404.
[62] D. Dobos, Electrochemical Data a Handbook for Electrochemists in Industry and Universities, Elsevier, 1975.
[63] K. Malek, M. Eikerling, Q. Wang, Z. Liu, S. Otsuka, K. Akizuki, M. Abe, Nanophase segregation and water dynamics in hydrated Nafion: Molecular modeling and experimental validation, J. Chem. Phys. 129 (2008) 20art no. 204702.
[64] V.I. Volkov, S.L. Vasilyak, I.-W. Park, H.J. Kim, H. Ju, E.V. Volkov, S.H. Choh, Water behavior in perfluorinated ion-exchange membranes, Appl. Magnetic Resonance 25 (1) (2003) 43–53.
[65] J. Kim, K.S. Kim, Structures, binding energies, and spectra of iso-energetic water hexamer clusters: extensive ab initio studies, J. Chem. Phys. 14 (109) (1998) 5886–5895.
[66] V.S. Bryantsev, M.S. Diallo, A.C.T. van Duin, W.A. Goddard III, Evaluation of B3LYP, X3LYP, and M06-class density functionals for predicting the binding energies of neutral, protonated and deprotonated water clusters, J. Chem. Theory Comput. 5 (2009) 1016–1026.